Molecular Recognition at the Dimer Interface of a Class Mu Glutathione Transferase: Role of a Hydrophobic Interaction Motif in Dimer Stability and Protein Function†

Judith A. T. Hornby,‡ Simona G. Codreanu,§ Richard N. Armstrong,*,§ and Heini W. Dirr*,‡

Protein Structure-Function Research Programme, School of Molecular and Cell Biology, University of the Witwatersrand, Johannesburg 2050, South Africa, and Departments of Biochemistry and Chemistry, Center in Molecular Toxicology, Vanderbilt University School of Medicine, Nashville, Tennessee 37232-0146

Received August 21, 2002; Revised Manuscript Received October 3, 2002

ABSTRACT: Cytosolic glutathione (GSH) transferases (GSTs) exist as stable homo- and heterodimers. Interactions at the subunit interface serve an important role in stabilizing the subunit tertiary structures of all GSH transferases. In addition, the dimer is required to maintain functional conformations at the active site on each subunit and the nonsubstrate ligand binding site at the dimer interface [Dirr, H. W. (2001) *Chem.-Biol. Interact. 133*, 19−23]. In this study, we report on the contribution of a specific intersubunit hydrophobic motif in rGSTM1-1 to dimer stability and protein function. The motif consists of the side chain of F56 from one subunit intercalated between helices 4 and 5 of the second subunit. Replacement of F56 with the hydrophilic side chains of serine, arginine, and glutamate results in a change in the structure of the active site, a marked diminution in catalytic efficiency, and alterations in the ability to bind nonsubstrate ligands. The mutations also affect the ability of the enzyme to bind GSH and the substrate analogue glutathione sulfonate. The functionality of rGSTM1-1 was disrupted to the greatest extent for the F56E mutant. Though mutations at this position do not alter the three-state equilibrium folding process for rGSTM1-1 (i.e., $N_2 \leftrightarrow 2I \leftrightarrow 2U$), destabilizing mutations at position 56 shift the equilibrium between the folded dimer (N_2) and the monomeric intermediate (I) toward the latter conformational state. The transition to the unfolded state (U) is not significantly affected. The folded monomeric intermediate is also observed by electrospray ionization mass spectrometry. The amount of the intermediate is dependent on protein concentration and the residue at position 56. Mutations at position 56 have little impact on the secondary structure and stability of the monomeric folding intermediate. The dimerization process is proposed to induce a conformational change in the loop containing F56, resulting in improved stability and increased affinity between the M1 subunits.

Protein−protein interactions are of fundamental importance to molecular biology because they determine a wide array of protein structures and functions. In addition to protein−protein complexes (e.g., antibody−antigen and protease−protein inhibitor complexes), many proteins are oligomeric due to the association of protein subunits. These protein−protein interactions are highly specific, displaying good geometric and chemical complementarity at the interacting surfaces. Hydrophobic and electrostatic interactions are the major forces stabilizing protein assemblies. These and other features of protein−protein interfaces are reviewed in refs *1*−*4*. The benefits for the existence of oligomeric proteins include reduced solvent-exposed surface areas and increased stability of the individual subunit structures, and the formation of novel functions at the interface (*5*). Interactions at the subunit interface of oligomeric proteins can assist in their folding to functional conformations. Studying engineered monomers that are stable but display compromised subunit−subunit associations can yield insight into the mechanisms by which a monomer obtains its final conformation in the oligomer. Such studies have been done with cro repressor (*6*), TIM (*7*), Rop (*8*), CRP (*9*), trp aporepressor (*10*), malate dehydrogenase (*11*), and ascorbate oxidase (*12*).

The cytosolic glutathione transferases (GSTs,[1] EC 2.5.1.18) have also been used to investigate the contribution of intersubunit interactions to protein stability and folding within a family of homologous dimeric proteins (*13*, *14*). Glutathione transferases exist as stable homo- and heterodimers (*15*) with a conserved archetypal fold (*16*−*18*). They constitute a superfamily of multifunctional proteins that can

† Supported by the University of the Witwatersrand, the South African Foundation for Research and Development, Wellcome Trust Grant 060799, Forgarty International Collaboration Award TW00779, and Grants R01 GM30910, P30 ES00267, and T32 ES07028 from the National Institutes of Health.

* To whom correspondence should be addressed. R.N.A.: e-mail, r.armstrong@vanderbilt.edu; fax, (615) 343-2921; telephone, (615) 343-2920. H.W.D.: e-mail, 089dirr@cosmos.wits.ac.za; fax, +27 11 403 1733; telephone, +27 11 717 6352.

‡ University of the Witwatersrand.

§ Vanderbilt University School of Medicine.

[1] Abbreviations: GST, glutathione transferase; ANS, 8-anilino-1-naphthalenesulfonate; CDNB, 1-chloro-2,4-dinitrobenzene; DTNB, dithiobis(2-nitrobenzoic acid); GdmCl, guanidinium chloride; GSH, reduced glutathione; GSO_3^-, glutathione sulfonate; PCR, polymerase chain reaction.

10.1021/bi020548d CCC: $22.00
Published on Web 11/07/2002

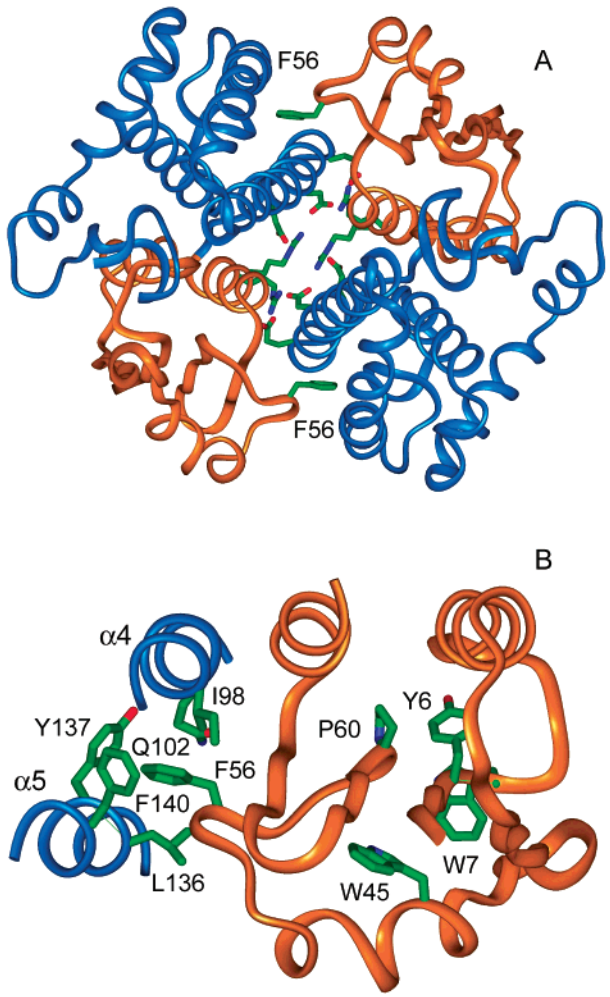

FIGURE 1: (A) Ribbon representation of the homodimeric mu class rGSTM1-1 viewed down the 2-fold axis (*47*). Domain I and domain II are represented by orange and blue ribbons, respectively. The side chains of F56 in the hydrophobic motif are indicated in stick representation. Charged, hydrophilic residues R77, R81, E90, D97, and E100 at the dimer interface are also shown in stick representation but not labeled. (B) Close-up of the hydrophobic interaction motif in rGSTM1-1. The side chains of Y6, W7, W45, F56, and P60 in domain I and I98, Q102, L136, Y137, and F140 in domain II are shown in stick representation.

be grouped into various species-independent gene classes (*16*, *18*). Although their dimer interfaces are not perfectly packed, they display good geometric complementarity which is essential for specific molecular recognition. Only subunits within a given GST gene class will associate to form dimers. Features at dimer interfaces are variable, but they suggest two major interface types: one that is jagged due to a specific hydrophobic intersubunit motif and another that is flat and more hydrophilic. Interactions at the subunit interface contribute to the stabilization of the subunit tertiary structures of GSTs, and the dimer is required to maintain functional conformations at the active site on each subunit and the nonsubstrate ligand binding (or ligandin) site at the dimer interface (*13*, *14*, *19*).

Dimeric proteins often tend to utilize large hydrophobic residues, e.g., Phe, Trp, and Tyr, that protrude from one subunit into the other to physically anchor the two subunits together (*20*). The glutathione transferases are an excellent example of this tendency. The structural features of the homodimeric rGSTM1-1 are shown in Figure 1. Each subunit consists of an N-terminal $\beta\alpha\beta\alpha\beta\beta\alpha$ domain (domain I) and a C-terminal all-helical domain (domain II). Intersubunit contacts occur between domain I of one subunit and domain II of the other. Contacts at either end of the interface are predominantly hydrophobic, whereas polar contacts form near the dimer 2-fold axis. The major hydrophobic contact between the subunits is that formed by the insertion of the phenyl ring of F56 from domain I of one subunit into a hydrophobic pocket in domain II of the second subunit. This particular interaction, sometimes termed the "lock-and-key motif", appears to have evolved relatively recently and is highly conserved in the class alpha, mu, and pi subfamilies (*21*).

Herein, the role of the hydrophobic motif at the dimer interface of class mu rGSTM1-1 in determining dimer stability and catalytic function is investigated. Disruption of the hydrophobic interaction was accomplished by replacing F56 with a series of hydrophilic side chains, including serine, arginine, and glutamate. The mutations lead to a significant disruption of the structure of the active site and a loss in catalytic activity. The loss of catalytic function of the mutants is not related to dissociation of the dimer but rather to a diminution in the ability to productively bind glutathione.

EXPERIMENTAL PROCEDURES

Materials. Ultrapure urea and GdmCl were purchased from ICN Biomedical Inc. (Irvine, CA) and Boehringer (Mannheim, Germany), respectively. All other chemical reagents were purchased from Sigma Chemical Co. (St. Louis, MO), and all the solutions were prepared and used on the same day. GSH concentrations were confirmed by titration with dithiobis(2-nitrobenzoic acid) (DTNB) (*22*). Stock solutions of 1-chloro-2,4-dinitrobenzene (CDNB) were prepared in ethanol (0.25 M). The final concentration of organic solvent in enzyme assays was 2.5%. All other reagents were analytical grade.

Generation of Expression Vectors. Site-directed mutagenesis was carried out by PCR using the single-stranded template DNA method as described by Kunkel (*23*). The pET20 expression vector (Novagen, Madison, WI) that encodes the native enzyme between the *Nde*I and *Hin*dIII restriction sites was used as a template for mutagenesis. DNA fragments encoding the three mutant enzymes (F56E, F56R, and F56S) were constructed by replacing the codon for phenylalanine (TTC) with that for glutamate (GAG), arginine (CGC), or serine (TCC). A new *Xba*I restriction site was engineered to facilitate the identification of the correct clones. The appropriate oligonucleotide primers were 39−48 bases long, phosphorylated, and complementary to the sequence, with the mismatched base in the middle. The resulting plasmids were used to transform bacterial strain DH5α, and colonies were selected for ampicillin resistance. The DNA fragments encoding the mutant enzymes were screened by DNA sequencing, to ensure that no secondary mutation occurred.

Expression and Purification of Mutant Proteins. F56 mutant enzymes of rGSTM1-1 were overexpressed in the BL21pLysS strain of *Escherichia coli*, according to the method of Parsons et al. (*24*) except that the cells were grown in enriched medium. The enzymes were purified by cation-exchange chromatography on a CM Sephadex column, using

10 mM sodium phosphate buffer (pH 7.0) as described by Hornby et al. (*25*). The protein concentrations of the dimeric mutants were determined spectrophotometrically using an extinction coefficient of 81 480 M^{-1} cm^{-1} at 280 nm (*25*).

Enzyme Kinetics. Mutant enzyme activities were assayed spectrophotometrically at 340 nm by monitoring the conjugation reaction between GSH and CDNB as previously described (*26*). All kinetic experiments were carried out in 0.1 M KH_2PO_4 (pH 6.5) and 25 °C. Kinetic constants k_{cat} and k_{cat}/K_m^{CDNB} were determined from initial velocity measurements using a fixed high concentration of GSH (30 mM for F56S, 60 mM for F56R, and 100 mM for F56E), while the concentration of the electrophilic substrate was varied. The values of K_m^{GSH} were determined using a fixed subsaturating concentration of CDNB (200 μM for F56R and F56S and 500 μM for F56E) and variable GSH. The mutant enzyme concentration was varied between 0.025 and 0.5 μM (monomer concentration). Each initial velocity was measured at least in triplicate, and all the rates are corrected for the background reaction. Each reaction mixture was incubated at 25 °C for 5 min prior to the addition of the electrophilic substrate. Initial velocities were analyzed using the program GraFit (Erithacus Software).

*Measurement of Inhibition Kinetic*s. The effect of glutathionesulfonic acid (GSO_3^-) on mutant enzyme activities was determined by monitoring the initial velocity of the reaction described above as a function of inhibitor concentration at two fixed concentrations of GSH (*27*). For all three mutant enzymes, the concentration of the electrophilic substrate was fixed at 200 μM. The GSH concentrations were 50 and 100 mM for the F56E mutant enzyme, 30 and 60 mM for the F56R mutant enzyme, and 5 and 10 mM for the F56S mutant enzyme. The inhibitor concentration was varied between 0 and 80 mM for the F56E and F56R mutant enzymes and between 0 and 15 mM for the F56S mutant. The data are plotted as $1/V$ as a function of inhibitor concentration for each GSH concentration, and the value of the inhibition constant ($-K_i$) is determined from the x-axis value at which the lines intersect. All inhibition data were analyzed using the program GraFit (Erithacus Software).

Size Exclusion Chromatography. The hydrodynamic behavior of the native enzyme and all three mutant enzymes was characterized by size exclusion chromatography through a Varian HPLC system, used along with a Tosohaas TSK-GEL G3000SWXL column (7.8 mm × 300 mm). Before chromatography was carried out, the proteins were dialyzed against the elution buffer and filtered through a 0.2 μm filter to remove particulate matter and any insoluble protein. Samples (20 μL) of the protein at concentrations ranging between 200 and 0.02 μM were injected and eluted at ca. 22 °C with 0.1 M KH_2PO_4, 0.1 M Na_2SO_4, 0.05% NaN_3 (pH 6.7) buffer at a flow rate of 0.5 mL/min in the absence or presence of 2 mM GSO_3^-. The elution of the protein was monitored continuously by the intrinsic protein fluorescence with excitation and emission wavelengths of 284 and 336 nm, respectively.

To determine the multimeric state of the eluted proteins, a standard calibration curve was generated by using a set of low-molecular mass proteins, which were run through the column under the same buffer conditions. The correlation coefficient (r) was 0.9993. The apparent molecular mass for each of the protein samples was obtained from the calibration curve by using linear regression analysis. The peak area, determined by HPLC Dynamax software, was used to calculate the percentage of dimeric and monomeric species for each sample. A plot of the percentage of dimer as a function of the total protein concentration was used to determine the dimer dissociation constant (K_D) for the F56R and F56S mutant enzymes. The experimentally determined K_D values were divided by a dilution factor of 12.5 ± 0.5. The dilution factor was employed since dilution of the protein sample occurs as the protein is eluted through the column. The dilution factor equals the peak width at half-height divided by the sample load volume (*28*, *29*).

Spectroscopic Measurements. Fluorescence measurements were taken with a Hitachi 850 fluorescence spectrophotometer (*25*). Steady state far- and near-UV CD spectra of the native enzyme and all three mutant enzymes were recorded on a JASCO J-720 spectropolarimeter equipped with a data processor. The protein concentration was 30 μM for both near- and far-UV CD measurements, prepared in 10 mM KH_2PO_4 (pH 7.0), which also contains 1 mM EDTA, 1 mM DTT, and 0.1 M KCl. Measurements were taken at 25° C in the presence or absence of GSO_3^- (5 mM). A quartz cell with a path length of 10 mm was used for near-UV CD (255−350 nm) measurements, while a cell with a path length of 1 mm was used for far-UV CD (180−255 nm) measurements. A total of 15 scans were recorded and averaged for each sample. All resultant spectra were corrected by subtracting the baseline.

Electrospray Ionization Mass Spectrometry. Noncovalent interactions from the dimer interface of the native and mutant enzymes were probed by a combination of electrospray ionization and time-of-flight mass spectrometry (ESI-TOF). ESI-TOF was performed using a Mariner mass spectrometer (PE Biosystems, Framingham, MA) equipped with a nanospray source. Protein samples were dialyzed against 4 mM ammonium acetate buffer that contains 5% methanol, at pH 6.7. Solutions were sprayed at room temperature, and the multiply charged positive ion spectra were recorded. Voltage dependence and temperature dependence experiments were performed to optimize the conditions for further spectrum acquisition. The final conditions consisted of an inlet capillary temperature of 160 °C and a capillary-skimmer offset potential of 200 V.

A concentration dependence experiment was performed to determine whether the intensities of the dimeric and monomeric species in the mass spectra are consistent with a monomer−dimer equilibrium in solution. The enzyme concentrations were varied from 2 to 100 μM. The fraction of dimer was calculated from the ESI spectra using the sum of the ion signal intensity and was plotted as a function of protein concentration.

Equilibrium Solvent-Induced Unfolding. All unfolding experiments were performed at 25 °C in 20 mM sodium phosphate buffer containing 0.1 M NaCl, 1 mM EDTA, and 0.02% NaN_3 (pH 6.5) as described previously (*25*). Protein, urea, and GdmCl concentrations were 0.2−2 μM, 0−8 M, and 0−6 M, respectively. Tryptophan fluorescence (excitation at 295 nm; emission at 335 and 355 nm for the folded and unfolded protein, respectively) and far- and near-UV CD ellipticities were used to monitor structural changes. ANS binding and enzyme activity were used as functional probes.

Table 1: Steady State Kinetic Parameters for Native and Mutant Enzymes

enzyme[a]	k_{cat} (s^{-1})	K_M^{CDNB} (μM)	k_{cat}/K_M^{CDNB} (M^{-1} s^{-1})	K_M^{GSH} (mM)	$K_i^{GSO3^-}$ (mM)
native	18 ± 2[b]	41 ± 4[b]	$(1.1 \pm 0.1) \times 10^6$[b]	0.16 ± 0.03	0.033 ± 0.004
F56S	90 ± 10	520 ± 90	$(1.7 \pm 0.2) \times 10^5$	20 ± 2	4.0 ± 0.5
F56R	24 ± 2	740 ± 160	$(3.3 \pm 0.2) \times 10^4$	54 ± 4	40 ± 2
F56E	7.8 ± 0.5	610 ± 100	$(1.3 \pm 0.2) \times 10^4$	74 ± 4	30 ± 2

[a] The concentrations of the enzyme used in the experiments were 0.025 μM for the native enzyme, 0.2 μM for F56S, and 0.5 μM for F56R and F56E. [b] Data from Parsons et al. (*24*).

Data Analysis. Analysis of the unfolding transitions and determination of conformational stability parameters were performed according to either a two-state model (*30*) ($N_2 \leftrightarrow 2U$) or a three-state model (*31*−*33*) ($N_2 \leftrightarrow 2I \leftrightarrow 2U$), where N_2 is the native dimer, I is a stable monomeric intermediate, and U is the unfolded polypeptide. Equilibrium unfolding data were fitted by nonlinear least-squares regression as described previously (*25*).

RESULTS

Functional Characterization of the F56S, F56R, and F56E Variants. The three mutant enzymes in which F56 was replaced with serine, arginine, or glutamate were expressed and purified in yields similar to that of the native enzyme. Although the mutants behave normally during the expression and purification, their catalytic characteristics are significantly compromised as indicated in Table 1. In initial kinetic studies, it was observed that the turnover number of the F56S and F56R mutants decreased with decreasing enzyme concentration, suggesting that at low concentrations the enzymes were dissociating to inactive monomers. However, if the enzymes are preincubated with the high (>1 mM) concentrations of GSH that are necessary for the assay, the kinetic constants exhibit relatively small changes as the enzyme concentration is decreased. The kinetic constants recorded in Table 1 were obtained under conditions (high enzyme concentration preincubated with GSH) where the catalytic efficiency was optimal.

The catalytic efficiency of all of the mutants is lower than that of the native enzyme with respect to k_{cat}/K_M^{CDNB}. However, the effect of the mutations on k_{cat} is quite variable, ranging from an increase with F56S to a decrease with F56E. The most pronounced effect of the mutations is seen in the increased values for K_M^{GSH}, suggesting that the mutations disrupt the GSH binding site. This conclusion is buttressed by the observation of a similar increase in the K_i of the competitive inhibitor, glutathione sulfonate (Table 1).

Spectroscopic Characterization of the Mutants. Fluorescence emission spectra for the folded and unfolded native and mutant proteins (excitation at 295 nm) are shown in Figure 2. The wavelength of maximum emission intensity of the mutants was similar to that for the native protein (335 nm). The maximum fluorescence intensities for the folded native enzyme and the F56S and F56R mutants are also similar, suggesting minor differences between the microenvironment of the tryptophan residues in these mutants and that of the native protein. The fluoresence intensity for the folded F56E mutant, on the other hand, is significantly increased, which is indicative of a tertiary structural perturbation at the tryptophan residues in this mutant. The unfolded native and mutant proteins display similar fluorescence

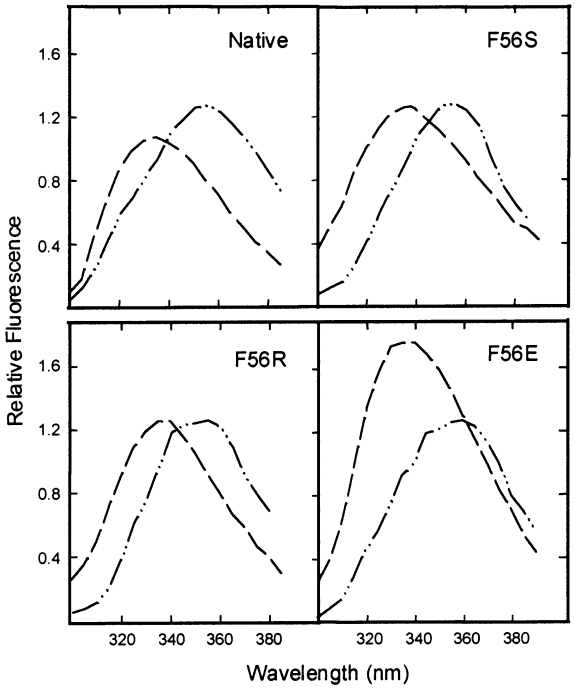

FIGURE 2: Fluorescence emission spectra of 1 μM native and mutant enzymes with excitation at 295 nm. The wavelengths of maximum emission intensity of the native, F56S, F56R, and F56E enzymes are 335, 338, 339, and 336 nm, respectively. Spectra of the proteins (− − −) in buffer and the unfolded proteins in 8 M urea (−••−) are shown.

spectra, indicating complete exposure of the tryptophan side chains to solvent (emission maximum at 355 nm).

The secondary and tertiary structures of the variants were monitored by far-UV CD (from 250 to 200 nm) and near-UV CD, respectively. The far-UV CD spectra of the mutants were similar to that observed for the native enzyme (*25*) and display two troughs at 210 and 222 nm due to the high helical content of the proteins (data not shown). The near-UV spectra are quite different and are consistent with the fluorescence data in indicating that the tertiary structure of the F56E mutant is more compromised than that of the other mutants (Figure 3A). The tertiary structure of F56E remains compromised even in the presence of GSO_3^-, whereas this ligand enables the other F56 mutants to regain a more nativelike CD spectrum (Figure 3B).

The native enzyme binds the anionic dye ANS, a molecule used to probe structural changes in the protein (*25*). The emission spectra for ANS in the presence of the native enzyme and F56 variants are shown in Figure 4. Unbound ANS has an emission maximum at 530 nm that shifts to the blue when the dye binds to the protein. The maximum emission wavelengths are 497 nm for the native enzyme, 481 nm for F56S, and 492 nm for F56R. The fluorescence of ANS bound to F56S and F56R is enhanced to a greater

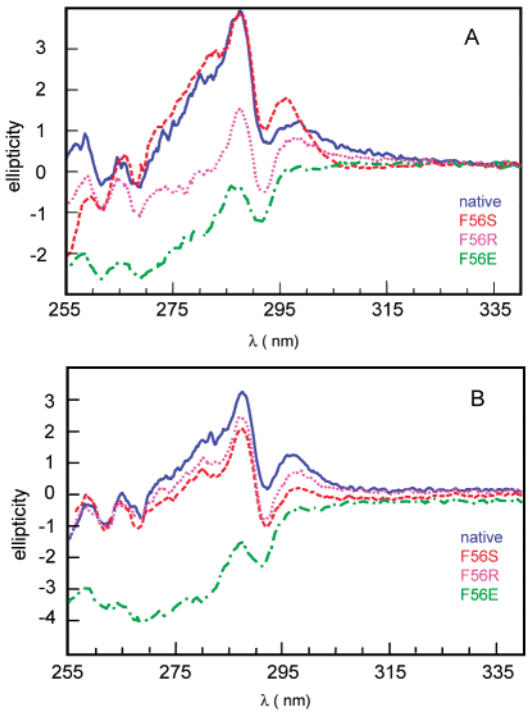

FIGURE 3: Near-UV CD spectra of the native enzyme and the F56S, F56R, and F56E mutants (A) in the absence and (B) in the presence of GSO_3^-.

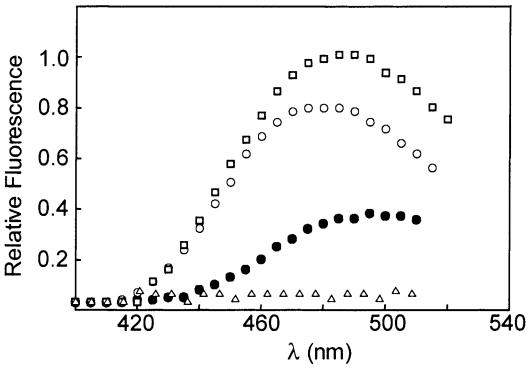

FIGURE 4: Fluorescence emission spectra of ANS bound to the native (●), F56S (○), F56R (□), and F56E (△) enzymes. Protein concentrations were 3.5 μM. Excitation was at 400 nm.

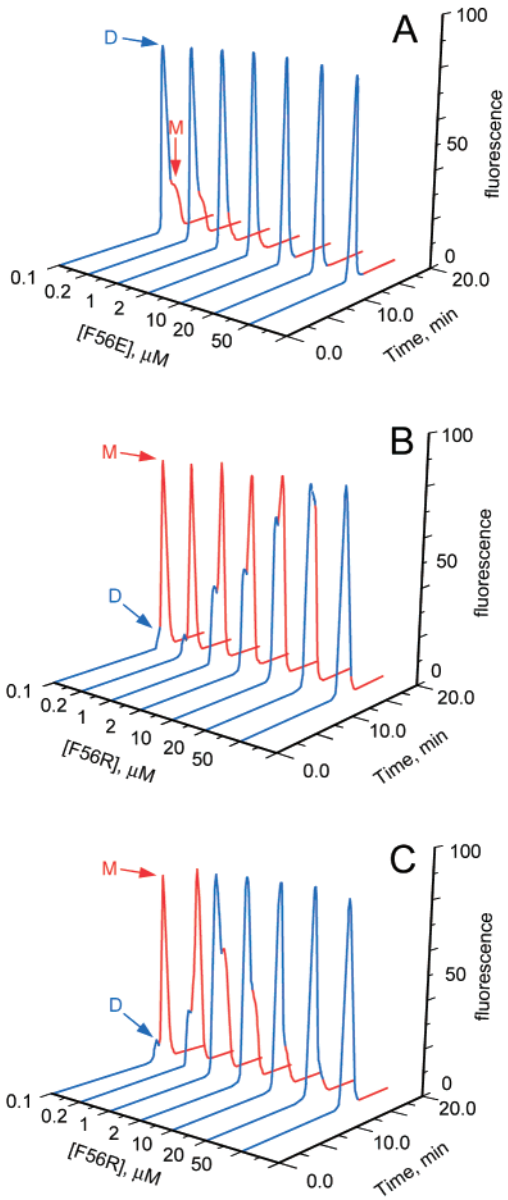

FIGURE 5: Protein concentration dependence of gel filtration profiles of (A) F56E, (B) F56R, and (C) F56R in the presence of 2 mM GSO_3^-. The protein concentration reported is that of the injected sample. The fluorescence signals were normalized to produce a uniform overall peak height.

extent than when bound to the native enzyme. No ANS binding is observed for the F56E mutant.

Gel Filtration Chromatography. Gel filtration chromatography was performed to assess the quaternary structure of the mutant enzymes under a range of protein concentrations. Both the native enzyme and the F56E mutant (Figure 5A) had elution volumes that corresponded to a molecular mass of 50 kDa, as expected for the dimeric protein. At a very low protein concentration, small amounts of the monomer were observed for both of these proteins as illustrated for the F56E mutant in Figure 5A. In contrast, the F56S and F56R mutants exhibited substantial amounts of monomer (molecular mass of 30 kDa) even at relatively high protein concentrations (10 μM) as illustrated for the F56R mutant in Figure 5B. If it is assumed that the monomer and dimer are at equilibrium during chromatography, then the integrated peak areas and chromatographic dilution factors can be used to estimate dissociation constants for the dimers of 0.9 ± 0.3 μM for F56R and 0.5 ± 0.2 μM for F56S. In the presence of the substrate analogue GSO_3^-, the monomer−dimer equilibria for F56R and F56S are shifted toward the dimer at low protein concentrations. This behavior is illustrated for F56R in Figure 5C.

Direct Observation of a Folded Monomer in the Gas Phase. The folding pathway of rGSTM1-1 has been proposed to involve a folded monomeric intermediate (I). Using gentle nanoelectrospray ionization conditions, it is possible to observe all three species postulated to exist along the equilibrium folding pathway. A folded monomer of rGSTM1-1 is readily observed as a minor species by electrospray ionization mass spectrometry performed at neutral pH as shown in Figure 6. The charge envelope of the folded monomer is centered at +10 and is distinctly different from that of the unfolded monomer centered at +26 and the folded dimer centered at +15 which is the major species at high protein concentrations. Small amounts of a trimer are also

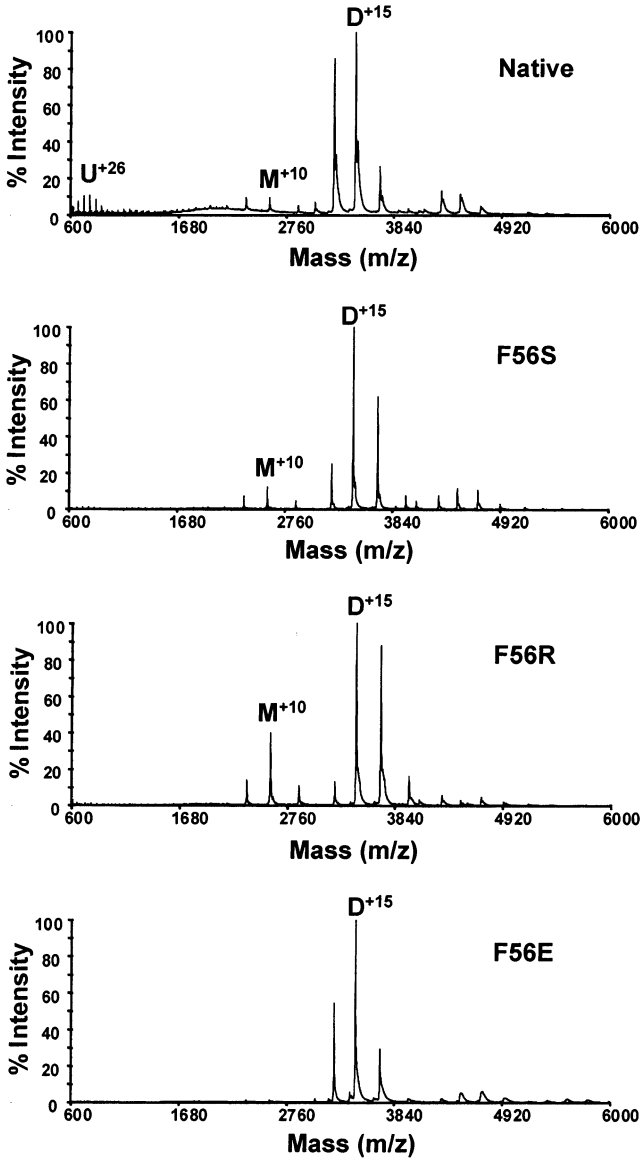

FIGURE 6: Detection of dimer, D, folded monomer, M, and unfolded monomer, U, by electrospray ionization mass spectrometry. The protein concentration in the sprayed samples was 20 μM.

observed due to nonspecific association of the dimer and monomer under the electrospray conditions. Notably, the amount of folded monomer detected by ESI-MS was significantly greater for the F56S and F56R mutants.

Under ideal conditions, ESI-MS should provide a snapshot of the species present in solution at equilibrium. The sensitivity of the instruments and complexities of the ionization and desolvation processes prevent the accurate determination of equilibrium constants. However, it is possible to examine the relative stability of noncovalent species (*34*−*36*). The protein concentration-dependent changes in the populations of monomer and dimer species indicate that the mutations have quite different effects on dimer stability. The fractions of dimer detected for the native enzyme and three mutants are compared under identical ionization conditions in Figure 7. The intensity of dimer ions present increases over the measured concentration range, consistent with the hypothesis that the dimers are in equilibrium with the free folded monomers in solution. The F56R and F56S mutants show a stronger tendency to form

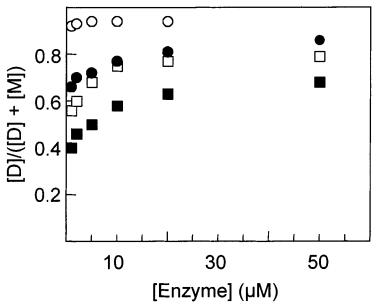

FIGURE 7: Concentration dependence of the fraction of dimeric species of rGSTM1-1 (●) and the F56E (○), F56S (□), and F56R (■) mutants observed by ESI-TOF mass spectrometry.

monomers at low concentrations. In contrast, the F56E mutant is the only protein that shows a constant fraction of dimer (ca. 0.95) across the entire concentration range, an observation consistent with a more stable mutant dimer. Inclusion of GSO_3^- in the solution substantially increases the amount of dimer observed in the ESI-TOF mass spectra of the native, F56R, and F56S proteins (data not shown). Even though solution equilibrium constants cannot be determined from these experiments, the results are in accord with and support the relative stability of the dimers observed in other experiments described herein.

Equilibrium Unfolding. As for the native enzyme, the recovery of structure and function of the mutant proteins from their unfolded states was in excess of 90%, as determined by fluorescence and enzyme activity, demonstrating the reversibility of the unfolding process. GdmCl-induced unfolding of the native and F56 mutant proteins is shown in Figure 8. The 222 nm CD transitions are monophasic for all the proteins, as shown in Figure 8B, indicative of a two-state unfolding process. This sigmoidal transition reports on the unfolding of the monomeric form of the enzyme (i.e., I ↔ U) and not on the dissociation event of the dimer (*25*). The coincidence of the CD transitions for the native and mutant proteins indicates that the monomeric states display similar conformational stability and $\Delta G(H_2O)$ values (see Table 2). The *m* values for the CD transitions (Table 2) compare well with that predicted for the monomeric native enzyme [4.8 kcal mol^{-1} (M GdmCl)$^{-1}$].

Denaturant-induced structural changes that occur prior to the dissociation of the GSTM1-1 dimer are reported by tryptophan fluorescence, enzyme activity, and ANS binding (*25*). At a protein concentration of 2 μM and in the absence of denaturant, the native enzyme and F56E mutant are expected to exist as dimers whereas F56S and F56R mutants are a mixture of monomer and dimer. The tryptophan fluorescence transitions, shown in Figure 8A, are not monophasic, indicating that unfolding is not a two-state process. The protein concentration dependence of the transitions was determined at 0.2 and 2 μM in an effort to discriminate between bimolecular (concentration-dependent dissociation, N_2 ↔ 2I) and unimolecular (concentration-independent unfolding, I ↔ U) events (*25*). Dissociation of the native rGSTM1-1 dimer occurs at low GdmCl concentrations (0−1.5 M, Figure 8B), and displays a dependence on protein concentration and loss of enzyme activity [data not shown; see Hornby et al. (*25*)]. The F56S and F56R mutants display very little concentration dependence between 0 and 1.5 M GdmCl (data not shown), whereas the fluorescence

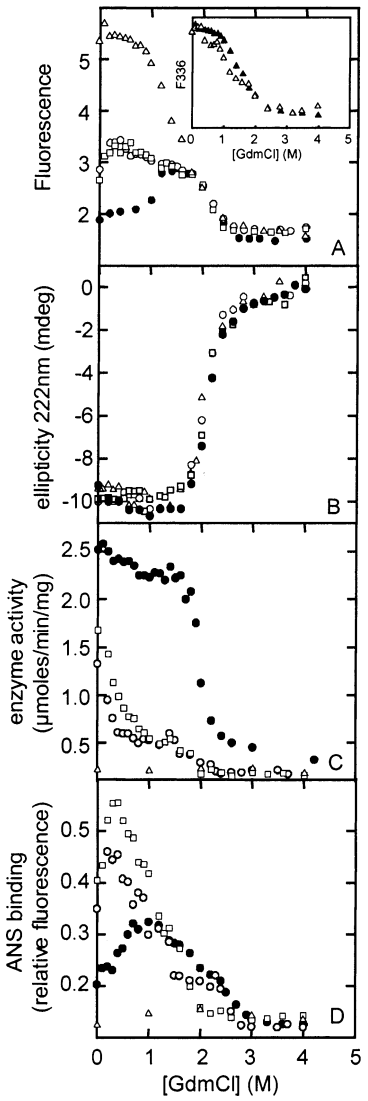

FIGURE 8: GdmCl-induced equilibrium unfolding curves for the native enzyme (●) and F56S (○), F56R (□), and F56E (△) in 20 mM sodium phosphate buffer (pH 6.5). The protein concentration was 2 μM: (A) fluorescence intensity at the emission wavelength peak for the folded proteins, (B) ellipticity at 222 nm, (C) loss of enzyme activity, and (D) change in the level of ANS binding. The inset in panel A illustrates the concentration dependence of the F56E mutant with respect to GdmCl-induced unfolding, monitored by fluorescence. The filled symbols represent protein at 2 μM and the empty symbols protein at 0.2 μM.

transition for F56E is concentration-dependent (Figure 8A inset). The shift in the fluorescence transitions to lower GdmCl concentrations for F56S and F56R indicates that their structures are more sensitive to denaturation than those of native rGSTM1-1 and F56E. These structural changes coincide with the loss of enzyme activity (Figure 8C). The fluorescence transitions observed at >1.5 M GdmCl are protein concentration-independent and correspond with the unfolding of the GST monomers as reported by CD. The loss of packing about the tryptophan residues is associated with the loss of secondary and tertiary structure upon unfolding.

The ANS binding behavior during the unfolding of the native and mutant rGSTM1-1 proteins is shown in Figure 8D. As mentioned above, native rGSTM1-1 and the F56S and F56R mutants bind ANS but F56E does not. Between 0 and 1.5 M GdmCl, the three former proteins display enhanced ANS binding that coincides with their initial tryptophan fluorescence changes. Enhanced ANS binding by rGSTM1-1 has been ascribed to the formation of a monomeric intermediate with a loosely packed tertiary structure (*25*). The unfolding of class sigma GSTS1-1, which does not have the hydrophobic interaction motif, also yields a monomeric intermediate, with enhanced ANS binding properties (*37*).

Table 2: Thermodynamic Parameters Obtained from both Urea and Guanidinium Chloride Equilibrium Denaturation of Native rGSTM1-1 and the F56S, F56R, and F56E Mutants Monitored by Fluorescence and Circular Dichroism[a]

	m_1 (dissociation) (kcal mol^{-1} M^{-1})	m_2 (unfolding) (kcal mol^{-1} M^{-1})	$\Delta G_{H_2O}{}^1$ (dissociation) (kcal/mol)	$\Delta G_{H_2O}{}^2$ (unfolding) (kcal/mol)
urea				
fluorescence[b]				
M1-1	1.0	3.4	10.8	16.5
F56E	0.9	2.5	9.9	15.7
CD				
M1-1		3.3		19.6
F56S		3.1		15.9
F56R		3.3		16.2
F56E		3.0		15.3
GdmCl				
fluorescence[b]				
M1-1	2.2	5.2	9.2	16.3
F56E	1.9	4.6	7.5	12.8
CD[c]				
M1-1		5.4		13.8
F56S		6.5		14.2
F56R		6.0		12.7
F56E		5.8		14.0

[a] Measurements were taken in 20 mM sodium phosphate buffer (pH 7.0) containing increasing concentrations of denaturants at 25° C, after equilibrium for at least 1 h. Regression coefficients of the individual fits were all greater than 0.967, and residuals show less than 5% deviation. [b] Fitted according to the three-state model ($N_2 \leftrightarrow 2I \leftrightarrow 2U$). See Experimental Procedures. [c] Fitted according to the two-state model [Pace et al. (*30*)]. Standard deviations for all values were calculated to be <20%.

The urea-induced unfolding transitions for the native rGSTM1-1 and its F56 mutants (data not shown) displayed the same trends as those obtained with GdmCl with the exception that the transitions occur, as expected, at higher denaturant concentrations. Data fitting of the unfolding transitions was not attempted for the F56S and F56R mutants due to the uncertainty regarding the initial concentrations of the dimer and monomer at 2 μM. However, since the F56E mutant exists predominantly as a dimer at this concentration, its fluorescence transition was fitted to a three-state model ($N_2 \leftrightarrow 2I \leftrightarrow 2U$) (*25*), as shown in Figure 9A for urea-induced unfolding. The relative populations of N_2, I, and U are shown in Figure 9B. Compared with the corresponding data for native GSTM1-1 (see Figure 10 in ref *25*), the F56E dimer is slightly less stable than the native dimer. The dissociation constant (K_d) values for the native and F56E proteins were calculated to be 0.012 and 0.055 μM, respectively. The low dissociation constants are consistent with their hydrodynamic properties on gel filtration chromatography (Figure 5A).

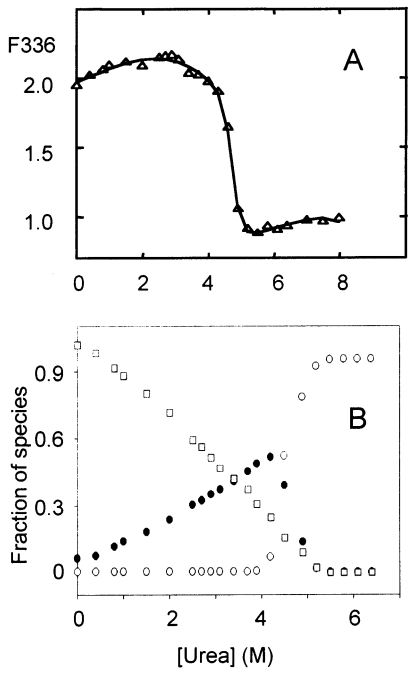

FIGURE 9: (A) Urea-induced unfolding of the F56E mutant of rGSTM1-1 monitored by fluorescence intensity at 336 nm. The fitted line was calculated according to the three-state fitting algorithm described in detail by Hornby et al. (*24*). Panel B describes the fraction of the folded dimer (□), monomeric intermediate (●), and unfolded (○) forms of the F56E mutant (2 μM) as a function of urea concentration at pH 6.5 and 25 °C, calculated for the tryptophan fluorescence data according to a three-state model ($N_2 \leftrightarrow 2I \leftrightarrow 2U$).

DISCUSSION

Hydrophobic Interaction Motif and Dimer Stability. Interactions at the subunit interface of cytosolic GSH transferases serve an important role in stabilizing the subunit tertiary structures and are required to maintain functional conformations at the active site on each subunit as well as the nonsubstrate ligand binding site at the dimer interface (*13*). Although the hydrophobic interaction common to the class alpha, mu, and pi enzymes is not essential for the dimerization of GST subunits (it is not a conserved motif in the canonical GST superfamily), mutations in this motif indicate that it contributes significantly to dimer stability and protein function (*14*, *19*).

The structure−function properties of these mutants indicate the disruptive nature of mutations at position 56 in the class mu enzyme. The most interesting result from this study is the fact that the nature of the disruption is highly dependent on the type of mutation that is introduced. Replacement of F56 with a serine or arginine residue significantly diminishes the stability of the dimer, shifting the dimer−monomer equilibrium toward the monomer at low protein concentrations. In contrast, the dimer stability of F56E is equivalent to that of the native enzyme. Unlike in rGSTM1-1, disruption of the dimer interface at F51 in the class alpha enzyme (hGSTA1-1) does not result in a stable monomeric intermediate (*14*). Instead, the folded dimer and unfolded monomers are highly populated in the single monophasic unfolding transition of the F51S mutant. Therefore, F56 in the class mu enzyme appears to play a greater role in maintaining a stable dimer than does the topologically equivalent F51 in class alpha GST. The monomers of the rGSTM1-1 F56 mutants display secondary structures and conformational stabilities similar to those of the native monomeric intermediate, indicating that the greatest impact of the mutations is on the tertiary structure of the rGSTM1-1 dimer.

Dimerization of glutathione transferases occurs after the formation of structured monomeric folding intermediates, as shown for hGSTA1-1 (*38*). Unlike in hGSTA1-1, which displays a highly concerted two-state folding and dimerization process at equilibrium (*39*), the stability of the class mu monomeric intermediate provides an opportunity to study the dimerization of rGSTM1-1 under equilibrium conditions. Although mutations at position 56 do not alter the three-state equilibrium folding pathway for rGSTM1-1 (i.e., $N_2 \leftrightarrow 2I \leftrightarrow 2U$), destabilizing mutations shift the equilibrium between the dimer N_2 and the folded monomeric intermediate I toward the latter state. The tertiary structure of the monomeric intermediate is not identical to that of the subunit in the dimer. Since the native and mutant intermediates appear to share a similar tertiary structure, the major structural difference between the subunit and intermediate most likely involves the loop region containing F56. Dimerization of M1 monomeric intermediates apparently induces the loop to assume a nativelike conformation, enabling the side chain of F56 to properly dock into the neighboring subunit, thus improving the complementarity and affinity between the M1 subunits.

Changes in the Nonsubstrate Binding Site. Disruption of the hydrophobic motif at the dimer interface of rGSTM1-1 affects the binding of the nonsubstrate ligand ANS. Unbound ANS has an emission maximum at ∼530 nm that shifts to the blue when the dye binds protein. The polarity of the ANS binding site determines the extent of the shift; the lower the polarity, the greater the blue shift. The ANS site in native rGSTM1-1 is not strictly hydrophobic as indicated by the fluorescence emission maximum of 495 nm for bound ANS (ref *25* and this work). This is compared with the emission maximum for ANS in water (530 nm) and a value of 454 nm for ANS bound to the highly hydrophobic site in apomyoglobin (*40*). The ANS binding site in rGSTM1-1 is more polar than that in hGSTA1-1 (*14*) and is apparently exposed to solvent. Because ANS fluorescence is quenched by water, the enhancement of the fluorescence intensity of protein-bound ANS is highly dependent upon its accessibility to water (*41*, *42*). The fluorescence enhancement of ANS when bound to native rGSTM1-1 is much lower in magnitude than that observed for other ANS-binding proteins (*41*, *43*, *44*), indicating a greater degree of exposure of ANS to solvent when bound to GSTM1-1. The polarity and degree of solvent exposure of the ANS site in rGSTM1-1 are reduced in the F56S and F56R mutants, whereas this binding site is abolished in the F56E mutant (Figure 5). Although the location of the ANS binding site(s) is unknown for class mu GSTs, it is reasonable to assume that it binds at or near the dimer interface. The anionic dye has been shown to bind the solvent-exposed cleft at the subunit interface of class alpha and pi enzymes (*45*, *46*).

Changes in the Active Site. The mutations at F56 can have a significant effect on the tertiary structure of the subunit in the dimer as evidenced by the substantial effect on the catalytic properties. These effects do not necessarily have a significant impact on dimer stability, depending on the type

of mutation. The diminished catalytic activity in the F56 mutants appears to be due to a defect in the ability of the enzyme to bind GSH and is the result of an altered conformation of the GSH binding site. The side chain of F56 is located in a loop (residues 47−60) between helix 2 and strand 3 at the active site (Figure 1) that is directly connected to the active site (Figure 1B). The loop itself plays an important role in binding GSH (*47*). Residues K49, N58, and L59 in the loop participate in hydrogen bonding interactions with bound GSH. At the end of the loop is P60, which is in the cis configuration and in van der Waals contact with Y6, a key residue involved in catalysis. Although the nature of the conformational changes induced by the F56 mutations is unknown, fluorescence and near-UV CD data indicate that the F56S and F56R mutations induce similar changes in the local environments of the tryptophan residues (W7 and W45) at the active site (see Figure 1). Both of these residues participate in hydrogen bonding interactions with GSH. Moreover, the binding of GSO_3^- or GSH can, to a certain extent, reverse these structural changes. Thus, the binding energy of the substrate is expended in reordering the active site and, as a consequence, can promote dimerization in the mutants.

At high concentrations of GSH, the mutant enzymes exhibit quite respectable turnover numbers. In fact, the F56S mutant has a turnover number for CDNB that is at least 4-fold larger than the turnover number of the native enzyme. It is known that the rate-limiting step in this reaction with the native enzyme is release of the product 1-(*S*-glutathionyl)-2,4-dinitrobenzene (*48*). Thus, the structural changes induced by mutations at F56 appear also to lead to enhanced rates of product release. The elevated K_M^{CDNB} for the mutants is almost certainly a manifestation of the fact that product release is no longer the rate-limiting step in catalysis.

The unique properties of the F56E mutant indicate that it adopts an alternate conformation that is structured for maintenance of the stability of the dimer at the expense of catalytic activity and the ability to bind ANS. The relative stability of the F56E dimer suggests that the side chain of E56 may interact with other residues in the neighboring subunit, resulting in a stable but non-nativelike conformation at the active site. The hydrophobic crevice between helices 4 and 5 in the neighboring subunit is composed of I98, V99, Q102, L136, Y137, and F140. The only side chain in this environment that could form a hydrogen bonding interaction with the carboxylate of E56 is the carboxamide of Q102. It remains to be determined if this or some other specific interaction is the source of the unique properties of the F56E mutant.

Conclusions. Mutations at the dimer interface of rGSTM1-1 have a pronounced effect on the stability of the dimeric protein and the conformation of the active site some 15−20 Å away from the site of mutation. The exact nature of the defects induced at the dimer interface and in the active site is highly dependent on the type of mutation and clearly indicates the importance of a properly configured interface to the functional properties of the enzyme. The structural consequences of these mutations are under investigation.

ACKNOWLEDGMENT

We thank Drs. David L. Hachey and Viet Nguen of the Mass Spectrometry Research Center at the Vanderbilt University School of Medicine for their assistance with the ESI-TOF MS experiments.

REFERENCES

1. Tsai, C.-J., Lin, S. L., Wolfson, H. J., and Nussinov, R. (1996) *Crit. Rev. Biochem. Mol. Biol. 31*, 127−152.
2. Xu, D., Lin, S. L., and Nussinov, R. (1997) *J. Mol. Biol. 265*, 68−84.
3. Jones, S., and Thornton, J. M. (1996) *Proc. Natl. Acad. Sci. U.S.A. 93*, 13−20.
4. Jones, S., and Thornton, J. M. (1997) *J. Mol. Biol. 272*, 121−132.
5. Larson, T. A., Olson, A. J., and Goodsell, D. S. (1998) *Structure 6*, 421−427.
6. Albright, R. A., Mossing, M. C., and Matthews, B. W. (1996) *Biochemistry 35*, 735−745.
7. Mainfroid, V., Terpstra, P., Beauregard, M., Frere, J.-M., Mande, S. C., Hol, W. G. J., Martial, J. A., and Goraj, K. (1996) *J. Mol. Biol. 257*, 441−456.
8. Munson, M., Balasubramanian, S., Fleming, K. G., Nagi, A. D., O'Brien, R., Sturtevant, J. M., and Regan, L. (1996) *Protein Sci. 8*, 1584−1593.
9. Kresl, J. J., Potempa, L. A., and Anderson, B. E. (1998) *Int. J. Biochem. Cell Biol. 12*, 1415−1426.
10. Shao, X. M., Hensley, P., and Matthews, C. R. (1997) *Biochemistry 36*, 9941−9949.
11. Breiter, D. R., Resnik, E., and Banaszak, L. J. (1994) *Protein Sci. 11*, 2023−2032.
12. Mei, G., DiVenere, A., Buganza, M., Vecchini, P., Rosato, N., and Finazzi-Agro, A. (1997) *Biochemistry 36*, 10917−10922.
13. Dirr, H. W. (2001) *Chem.-Biol. Interact. 133*, 19−23.
14. Sayed, Y., Wallace, L. A., and Dirr, H. W. (2000) *FEBS Lett. 465*, 169−172.
15. Mannervik, B., and Jensson, H. (1982) *J. Biol. Chem. 257*, 9909−9912.
16. Dirr, H. W., Reinemer, P., and Huber, R. (1994) *J. Mol. Biol. 243*, 72−92.
17. Wilce, C. J., and Paker, M. W. (1994) *Biochim. Biophys. Acta 1205*, 1−18.
18. Armstrong, R. N. (1997) *Chem. Res. Toxicol. 10*, 2−18.
19. Stenberg, G., Abdalla, A. M., and Mannervik, B. (2000) *Biochem. Biophys. Res. Commun. 271*, 59−63.
20. Jones, S., and Thornton, J. M. (1995) *Prog. Biophys. Mol. Biol. 63*, 31−65.
21. Ji, X., von Rosenvinge, E. C., Johnson, W. W., Tomarev, S. I., Piatigorsky, J., Armstrong, R. N., and Gilliland, G. L. (1995) *Biochemistry 34*, 5317−5328.
22. Ellman, G. L. (1959) *Arch. Biochem. Biophys. 82*, 70−74.
23. Kunkel, T. A., Roberts, J. D., and Zakour, R. A. (1987) *Methods Enzymol. 154*, 367−382.
24. Parsons, J. F., Xiao, G., Gilliland, G. L., and Armstrong, R. N. (1998) *Biochemistry 37*, 6286−6294.
25. Hornby, J. A. T., Luo, J.-K., Stevens, J. M., Wallace, L. A., Kaplan, W., Armstrong, R. N., and Dirr, H. W. (2000) *Biochemistry 39*, 12336−12344.
26. Habig, W. H., and Jakoby, W. B. (1981) *Methods Enzymol. 77*, 398−405.
27. Dixon, M. (1953) *Biochem. J. 55*, 170.
28. Manning, L. R., Jenkings, W. T., Hess, J. R., Vandegriff, K., Winslow, R. M., and Manning, J. M. (1996) *Protein Sci. 5*, 775−781.
29. Dorfman, R., and Walsh, P. N. (2001*) J. Biol. Chem. 276*, 6429−6438.
30. Pace, C. N., Shirley, B. A., and Thornton, J. A. (1989) in *Protein Structure: A Practical Approach* (Creighton, T. E., Ed.) pp 311−330, Oxford University Press, Oxford, U.K.
31. Gloss, L. M., and Matthews, C. R. (1998) *Biochemistry 37*, 15990−15999.
32. Park, Y.-C., and Bedouelle, H. (1998) *J. Biol. Chem. 273*, 18052−18059.
33. Park, Y.-C., and Bedouelle, H. (1999) *J. Mol. Biol. 286*, 563−577.
34. Li, Y.-T., Hsieh, Y.-L., Henion, J. D., Senko, M. W., McLafferty, F. W., and Ganem, B. (1993) *J. Am. Chem. Soc. 115*, 8409−8413.

35. Light-Wahl, K. J., Schwarts, B. L., and Smith, R. D. (1994) *J. Am. Chem. Soc. 116*, 5271−5278.
36. Fligge, T. A., Reinhard, C., Harter, C., Wieland, F. T., and Przybylski, M. (2000) *Biochemistry 39*, 8491−8496.
37. Stevens, J. M., Hornby, J. A. T., Armstrong, R. N., and Dirr, H. W. (1998) *Biochemistry 37*, 15534−15541.
38. Wallace, L. A., and Dirr, H. W. (1999) *Biochemistry 38*, 16686−16694.
39. Wallace, L. A., Sluis-Cremer, N., and Dirr, H. W. (1998) *Biochemistry 37*, 5320−5328.
40. Stryer, L. (1965) *J. Mol. Biol. 13*, 482−495.
41. Kirk, W. R., Kurian, E., and Prendergast, F. (1996) *Biophys. J. 70*, 69−83.
42. Matulis, D., and Lovrien, R. (1998) *Biophys. J. 74*, 422−429.
43. Nishihira, J., Ishibashi, T., Sakai, M., Tsuda, S., and Hikichi, K. (1993) *Arch. Biochem. Biophys. 302*, 128−133.
44. Ory, J. J., and Banaszak, L. J. (1999) *Biophys. J. 77*, 1107−1116.
45. Sluis-Cremer, N., Naidoo, N. N., Kaplan, W. H., Manoharan, T. A., Fahl, W. E., and Dirr, H. W. (1996) *Eur. J. Biochem. 241*, 484−488.
46. Sayed, Y., Hornby, J. A., Lopez, M., and Dirr, H. (2002) *Biochem. J. 363*, 341−346.
47. Ji, X., Zhang, P., Armstrong, R. N., and Gilliland, G. L. (1992) *Biochemistry 31*, 10169−10184.
48. Johnson, W. W., Liu, S., Ji, X., Gilliland, G. L., and Armstrong, R. N. (1993) *J. Biol. Chem. 268*, 11508−11511.

BI020548D